

# Luminous Matter Distribution, Bulk Flows and Baryon Contents in Cosmological Models with a Local Void

Kenji TOMITA<sup>\*)</sup>

*Yukawa Institute for Theoretical Physics, Kyoto University, Kyoto 606-8502*

First galaxy formation is discussed from the viewpoint of hierarchical clustering theory and it is shown that inhomogeneous models with a local void may be compatible with the observed homogeneity of galactic distributions given by recent redshift surveys, because of the difference in the feedback system of galaxy formation in the inner and outer regions. Next it is shown that the observed inhomogeneity of two-point correlations of galaxies can be explained in these models using numerical simulations, and the natural appearance of bulk flows for an off-central observer is shown. Finally the inhomogeneity of baryon contents is discussed from the viewpoint of our inhomogeneous models.

## §1. Introduction

Under the assumption of spatial homogeneity, the cosmological parameters have been determined using important observations such as the [magnitude  $m$  - redshift  $z$ ] relation of type Ia SN<sup>1), 2), 3), 4)</sup> and the anisotropy of cosmic microwave background radiation (CMB)<sup>5), 6), 7), 8), 9)</sup>, and it was found that models with dominant cosmological constant is fit for SN data and the flat models are fit for CMB data.

On the other hand, the present author<sup>10)</sup> considered the models with a local void on scales of  $\sim 200$  Mpc, in order to explain the existence of large-scale bulk flows which were discovered by Hudson et al.<sup>11)</sup> and Willick,<sup>12)</sup> and showed<sup>13), 14), 15)</sup> that the zero- $\Lambda$  or small- $\Lambda$  models with flat space in the outer region are consistent with the data of type Ia supernovae (especially the recent data for  $z = 1.7$ <sup>16)</sup>), and with the CMB anisotropy. So these models are competent for explaining the cosmological observations in spite of the small realization probability of their large-scale void. Here the void means a low-density region with respect to the total matter, which consists mainly of the dark matter.

The homogeneity of galactic distributions shown by recent redshift surveys may support the homogeneous models, but does not necessarily deny the inhomogeneous models with a local void, in which the galactic number densities in the inner and outer regions may be comparable owing to the larger suppression of galaxy formation in the outer region.

In this paper we consider in §2 the process of galaxy formation and observational aspects in inhomogeneous models from the viewpoint of theories of hierarchical galaxy formation. There we discuss the observed galactic distributions in connection with a local void and the two-point correlation which reflects the inhomogeneous structure of our models. In §3, we describe the models with a local void using numerical simulations, and in §4, we analyze the theoretical two-point correlations ( $\xi^I$

---

<sup>\*)</sup> E-mail address: tomita@yukawa.kyoto-u.ac.jp

and  $\xi^{\text{II}}$ ) in the inner and outer regions, respectively, and show the ratio  $\xi^{\text{I}}/\xi^{\text{II}}$  is consistent with the observed ratio. In §5, we derive the bulk flows for the an off-center observer and show that they are consistent with the observed ones. In §6 we discuss the inhomogeneity of baryon contents from our viewpoint. Section 7 is dedicated to concluding remarks.

## §2. Galaxy formation and observational aspects

Modern theories of galaxy formation had a great deal of progress in understanding of galactic properties under the assumption of cold dark matter (CDM) in hierarchical clustering cosmologies. It was assumed that galaxies form when gas cools and condenses in dark matter halos which merge in their evolutionary process. The key point in these theories was the energy release from stars as “negative feedback” on the gas and star formation, which was proposed by White and Rees<sup>17)</sup> and developed by White and Frenk.<sup>18)</sup>

Recent works of galaxy formation, including the process of feedback, have used two important methods, semi-analytic method and numerical simulations. The first is directly connected with the above two pioneering works and take into account the feedback in details, but in simplified (spherically symmetric) situations. The merger history of dark matter halo is treated using either the statistical method (Kauffmann et al.,<sup>19)</sup> Cole et al.,<sup>20), 21)</sup> Somerville and Primack<sup>22)</sup>) or the  $N$ -body simulations (Kauffmann, Nusser and Steinmetz,<sup>23)</sup> Kauffmann, Colberg, Diaferio and White,<sup>24)</sup> Benson et al.,<sup>25)</sup> Somerville et al.<sup>26)</sup>). The second one treats not only the merger history using the  $N$ -body simulations, but also the feedback process and star formation using gas dynamical simulations (Cen and Ostriker,<sup>27)</sup> Katz, Weinberg and Hernquist,<sup>28)</sup> Frenk et al.,<sup>29)</sup> Kay et al.<sup>30)</sup>). This method has the advantage that no artificial symmetries need to be imposed, but the disadvantage that the treatment is not so transparent and there are unrealistic limits on the dynamic range of resolved structures, though the resolution is being improved with the use of high-speed supercomputers. In the following let us first show the outline of recent treatments of galaxy formation on the basis of Kauffmann et al.’s semi-analytic method, and next consider how we should treat galaxy formation in the present models with a local void.

### 2.1. Galaxy formation in homogeneous models

Kauffmann et al.’s semi-analytic models<sup>24)</sup> are given in the combination of the  $N$ -body simulations and the analytic approach to the star formation and supernova feedback. The  $N$ -body simulations are performed using the cluster normalization by determining  $\sigma_8$ , the dispersion of density perturbations within  $8h^{-1}$  Mpc spheres in two CDM models: SCDM ( $\tau$ model) and  $\Lambda$ CDM with

$$(\Omega_0, \lambda_0, h, \sigma_8, \Gamma, f_b) = (1.0, 0.0, 0.5, 0.6, 0.21, 0.1), (0.3, 0.7, 0.7, 0.7, 0.9, 0.21, 0.15),$$

respectively, where  $\Gamma$  is the shape parameter of the power spectrum and  $f_b$  is the baryon factor ( $\equiv \Omega_b/\Omega_0$ ).

The merging history of dark matter halos is constructed using the halo catalogues

which consist of halos larger than the least stable system (containing 10 particles). In each halo there is a central particle indicating the central galaxy onto which gas in a halo falls and where stars form. The central galaxy in a halo is the central galaxy in its most massive progenitor and the central galaxies in less massive progenitor are satellites in the halo. These galaxies also grow from small galaxies to larger galaxies through merging.

The physical properties of galaxies are determined by gas cooling, star formation, supernova feedback, dust extinction, etc. The most important ones of them are star formation and supernova feedback. The star formation rate of the form

$$dM_*/dt \ (\equiv \dot{M}_*) = \alpha M_{\text{cold}}/t_{\text{dyn}} \quad (2.1)$$

is assumed, where  $\alpha$  is a free parameter,  $t_{\text{dyn}}$  is the dynamical time of the galaxy, and  $M_*$  and  $M_{\text{cold}}$  are the total masses of stars and cold gas in the halo, respectively.

The energy ejected by supernova explosion into the interstellar medium is used to reheat the cold gas to the virial temperature. The reheating rate is expressed in the form

$$dM_{\text{reheat}}/dt = \epsilon \frac{4}{3} \dot{M}_* \eta_{\text{sn}} E_{\text{sn}} / V_c^2, \quad (2.2)$$

where  $\eta_{\text{sn}}$  is the number of supernovae per solar mass of stars ( $= 5 \times 10^{-3}/M_{\odot}$ ,  $E_{\text{sn}}$  is the kinetic energy of the ejection from each supernova ( $\cong 10^{51}$  erg),  $\epsilon$  is a free parameter representing a fraction of this energy used to reheat cold gas, and  $V_c$  is the circular velocity of galaxies.

The evolution of distributions of dark matter halos and galaxies within them is determined using Eqs. (2.1) and (2.2), when we specify the free parameters  $\alpha$  and  $\epsilon$ , and the present distributions can be compared with the observations in the form of luminosity functions, Tully-Fisher relations and the two-point correlations. In order to choose the best values of  $\alpha$  and  $\epsilon$ , a normalization condition is imposed: a fiducial reference galaxy (which is defined as a central galaxy with  $V_c = 220 \text{ km s}^{-1}$ ) should satisfy the *I*-band Tully-Fisher relation. Then the set  $(\alpha, \epsilon)$  is given as (0.07, 0.15) and (0.1, 0.03) for SCDM ( $\tau$ CDM) and  $\Lambda$ CDM models, respectively. These values mean that the SCDM model has smaller star formation and larger feedback than the  $\Lambda$ CDM model. For these sets, both the SCDM and  $\Lambda$ CDM models have luminosity functions, Tully-Fisher relations and two-point correlations consistent with the observed ones. In addition to the feedback due to supernova explosion, the photoionization and heating due to the ultraviolet radiation also contributes to the feedback. <sup>31), 32), 33)</sup>

## 2.2. Galaxy formation in the models with a local void

In these models the total matter (consisting mainly of dark matter) has different uniform densities in the inner region ( $r < r_b$ ) and the outer region ( $r > r_b$ ), while the distributions of the luminous matter (consisting of galaxies) may be nearly uniform through the two regions, if the star formation and the feedback effect in the two regions work well in a cooperative manner.

Let us assume for instance that the outer region is represented by the Einstein-de Sitter model and the inner region is by an open model with  $(\Omega_0, \lambda_0) = (0.3, 0)$ . Then

we can have  $(0.07, 0.15)$  as the set  $(\alpha, \epsilon)$  in the outer region. Because the model in the inner region is similar to that in the low-density model with  $(\Omega_0, \lambda_0) = (0.3, 0.7)$ , we can have  $(\alpha, \epsilon) = (0.1, 0.03)$  approximately, in the central part of the inner region, say  $r \leq r_{\text{in}} (\leq r_b)$ .

In the transient region of  $r_{\text{in}} \leq r \leq r_b$ , the values of the set  $(\alpha, \epsilon)$  change gradually from the outer  $(0.3, 0)$  to the inner  $(0.1, 0.03)$ . The strong photoionization by UV radiation from the outer region to the inner region may play an effective role to prevent small galaxies from forming and so growing by merging in this region. So the number density of forming galaxies is small there, compared with the densities in the outer and inner regions.

Galaxies formed in the transient region enter the outer region thereafter, colliding with the galaxies there, since the inner expanding velocities are larger than the outer velocities. At the present epoch the boundary ( $r = r_{\text{in}}$ ) of the inner central region reaches the boundary  $r = r_b$  of the outer region, so that the number densities of galaxies in the outer and inner regions may be nearly equal, as shown in Fig. 1. At present, however, we cannot determine the position of  $r = r_{\text{in}}$  accurately, since the studies on the dependence of rates of star formation, supernova explosion and the UV radiation on the background models have not been established yet.<sup>34)</sup> Depending on the rates and the position of the central part ( $r < r_{\text{in}}$ ), the various large-scale structures may appear around the boundary ( $r = r_b$ ). It is estimated from simple simulations that, if the radial distance for  $r_{\text{in}} \leq r \leq r_b$  is about 1/4 of that for  $0 \leq r \leq r_b$  on the comoving scale, the two regions are smoothly connected later.

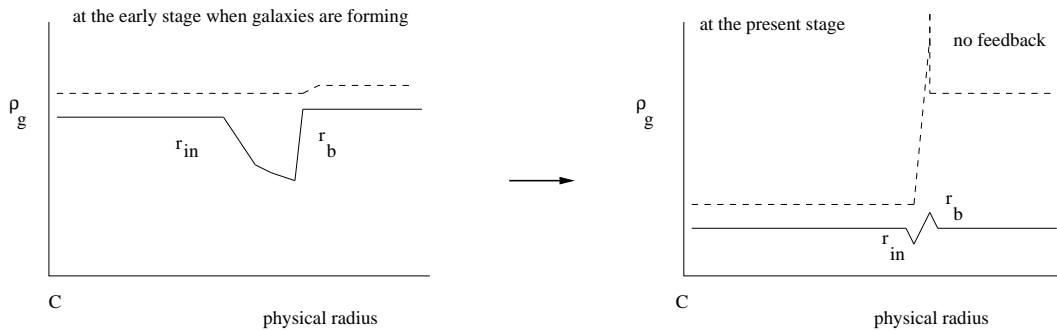


Fig. 1. The schematic evolution of galactic density  $\rho_g$  around the boundary  $r_b$ . The dashed lines denote the case of no feedback.

Here we have an important prediction that around the boundary there must be many active galaxies which were born as a result of the frequent collision of galaxies, even if the distribution of galaxies is smooth there owing to the strong feedback.

It is important to investigate the evolution of luminous matter by numerical simulations, taking into account the above complicated processes including cooling, star formation, supernova feedback and heating by UV radiation, but they are much beyond the scope of this paper.

### 2.3. Observed galactic distributions

Here we look over the present observed situation in galactic distributions from the viewpoint of our inhomogeneous models.

#### 2.3.1. Dependence on the observer's position

Several redshift surveys have suggested the existence of a low density region or a local void with the radius  $\sim 300h$  Mpc ( $H_0 = 100h$  km sec $^{-1}$  Mpc $^{-1}$ ).<sup>35), 36), 37), 38)</sup> Latest surveys (2dF and SDSS) show that the galactic distributions within the radius  $\sim 600h$  Mpc are homogeneous on the whole, though they include various large-scale structures. So the observed distributions seem to be consistent with homogeneous cosmological models. However inhomogeneous models with a local void also may be compatible with the above surveys, because

(1) the number density of galaxies in the inner low-density region and the outer high-density region can be comparative in these models also, as discussed in the previous subsection, and

(2) part of observed large-scale structures which are regarded as independent may represent the correlated structures near the boundary. For an observer in the center these correlated structures have an equal redshift and can easily be distinguished. For us (off-center observers), however, they have the direction-dependent redshifts and are confused with other uncorrelated structures. When we superpose the redshift histograms in various directions in the north and south, off-central observers may see the structures there as independent ones at the different distances.

#### 2.3.2. Active galaxies around the boundary

From a recent study for spectral types of galaxies in the 2dF survey (Madgwick et al.<sup>39)</sup>), it was found that there are many active galaxies in the redshift region with which corresponds to the boundary  $r = r_b$ . These galaxies may have been born as the result of the above-mentioned collision of galaxies around the boundary. Similar analyses for the spectral types of galaxies are necessary for the SDSS survey to clarify the astrophysical situation around the boundary.

#### 2.3.3. Two-point correlation

The apparent distribution of luminous matter is not so useful to study the background model consisting mainly of dark matter, because of much complicated processes of formation and evolution of galaxies. The two-point correlations of galaxies, on the other hand, depend mainly on the background model, at least for less luminous galaxies in the homogeneous regions. So it may be significant that we use the correlations to study the distribution of dark matter also.

Recently the large-scale redshift surveys have brought us the valuable information about the spatial dependence of the two-point correlations of galaxies in the region of  $z < 0.1$ . Using the NGP + SGP data in the 2dF surveys, Norberg et al.<sup>40)</sup> derived the correlation length  $r_0$  in samples with the various parameters ranges (cf. Table 1 and Fig. 3 in their paper). The observed correlation length increases with the absolute magnitude as

$$r_0 = 4.14 \pm 0.64, 4.43 \pm 0.45, \dots, 9.38 \pm 1.48$$

for  $(M_{bJ} - 5 \log_{10} h, z) = (-18.0 \sim -18.5, 0.010 \sim 0.080), (-18.5 \sim -19.0, 0.013 \sim$

0.104), ...,  $(-21.5 \sim -22.5, 0.059 \sim 0.28)$ , respectively, where  $M_{bJ}$  is the  $b$ -band absolute magnitude. The other data in SSRS2, EPS and Stromlo data also show the trend similar to that in 2dF survey, as in Fig. 3 in Norberg et al.'s paper<sup>40)</sup>. The luminosity dependence of  $r_0$  in these samples seems to be consistent with that which was discussed in the hierarchical galaxy formation theories.

According to the recent theory on the galactic distribution (Benson et al.<sup>25)</sup>,  $r_0$  increases with the increase of  $-M_{bJ}$  for  $-(M_{bJ} - 5 \log_{10} h) > 21$ , while  $r_0$  is constant or slightly decreases for  $-M_{bJ}$  for  $-(M_{bJ} - 5 \log_{10} h) < 21$ . The observed value of  $r_0$  increases with the increase of  $-M_{bJ}$  even for  $-(M_{bJ} - 5 \log_{10} h) < 21$ . Quantitatively it increases by a factor of about 1.5 for the interval of  $(M_{bJ} - 5 \log_{10} h) = -18 \sim -21$ . The two-point correlation  $\xi \propto r_0^\gamma$  ( $\gamma \approx 1.7$ ) change by a factor 2.0 for this interval. We can interpret this change to represent the redshift dependence (or the spatial inhomogeneity) of  $r_0$  or  $\xi$  in the region of  $z = 0.010 \sim 0.280$ . The boundary ( $z \sim 0.07$ ) of a local void we consider is included in this region.

From the data of the SDSS survey, Zehavi et al.<sup>41)</sup> derived the correlation length  $r_0$  in three samples :

$$r_0 = 7.42 \pm 0.33, 6.28 \pm 0.77 \text{ and } 4.72 \pm 0.44$$

for  $(M_r^*, z) = (-23.0 \sim -21.5, 0.100 \sim 0.174)$ ,  $(-21.5 \sim -20.5, 0.052 \sim 0.097)$ , and  $(-20.0 \sim -18.5, 0.027 \sim 0.051)$ , respectively (cf. Table 2 and Fig. 16 in their paper). Their result also shows the change in  $r_0$  by the factor of about 1.33 in the interval of  $M_r^* = -21.5 \sim -18.5$ . This change can be interpreted as the redshift dependence of  $r_0$  in the interval of  $z = 0.027 \sim 0.097$ . Our boundary ( $z \sim 0.07$ ) is included similarly in this interval.

In order to explain these spatial change in  $r_0$  or  $\xi$ , let us study inhomogeneous models with a local void in the following sections using simple simulations.

### §3. Numerical inhomogeneous models

In previous papers I used models with a local void consisting of homogeneous inner and outer regions with a singular shell or an intermediate self-similar region. In order to study the evolution of nonlinear perturbations and their two-point correlations in these regions, I derived in this section numerical inhomogeneous models using the method of  $N$ -body simulation, by considering a spherical low-density region in the background homogeneous models. The background model parameters are expressed as  $H_0, a_0, \Omega_0$  and  $\lambda_0$ , where they are the Hubble constant, the scale factor, the density parameter and the cosmological-constant parameter at the present epoch  $t = t_0$ , respectively, and the spatial curvature is  $K = a_0^2 H_0^2 (\Omega_0 + \lambda_0 - 1)$ . Proper radial distance  $R$  at  $t_0$  is related to the radial coordinate  $r$  by  $R = a_0 r$ . As the background models we took following three cases:  $(\Omega_0, \lambda_0, h) =$  (1) Einstein-de Sitter model (1.0, 0.0, 0.5), (2) Open model (0.6, 0.0, 0.6) and (3) Flat nonzero- $\Lambda$  model (0.6, 0.4, 0.6).

The  $N$ -body simulation was performed using the tree-code exploited by Suto and Sugimoto, in which the periodic condition is imposed, and the initial perturbed state was determined using COSMICS. Here  $N = 2.1 \times 10^6$  and the particle mass  $M$  is  $M = 5.7, 2.9$  and  $2.9 \times 10^{13} M_\odot$  for the above three cases (1), (2) and (3),

respectively. The softening radius is 1 Mpc for all cases. The periodic condition was given at  $|x^1| = |x^2| = |x^3| = r_p$ , where  $R_p \equiv a_0 r_p = 300/h$  Mpc and  $r \equiv [(x^1)^2 + (x^2)^2 + (x^3)^2]^{1/2}$ .

The initial condition was set at  $t = t_i$  at which  $z = z_i$  ( $= 15.5$ ), in the form of displacements  $\delta x^k$  and velocities  $v^k$  of  $N$  particles ( $k = 1, 2, 3$ ). After the initial condition in the homogeneous case was given, a low-density region was introduced at the initial epoch by changing the particle positions  $x^k$  in the inner region ( $r < r_b$ ) and the intermediate region ( $r_b < r < r_{b1}$ ) as follows:

$$x^k = (x^k)_{\text{hom}} \times \begin{cases} (1+d) & \text{for } r < r_b, \\ \left[ 1 + d \left( \frac{1}{r_b} - \frac{1}{r_{b1}} \right) / \left( \frac{1}{r} - \frac{1}{r_{b1}} \right) \right] & \text{for } r_b \leq r < r_{b1}, \end{cases} \quad (3.1)$$

and  $x^k = (x^k)_{\text{hom}}$  for  $r > r_{b1}$  (see Fig. 2). Here  $(x^k)_{\text{hom}}$  represent the particle positions in the homogeneous case and  $d$  is a constant expansion factor adjusted so as to give the expected density parameter and average expansion rate in the inner region. The intermediate region was introduced to make smooth the change in the density and velocity of particles near the boundary. Here we treated mainly the case of  $R_b \equiv a_0 r_b = 180/h$  Mpc and  $R_{b1} \equiv a_0 r_{b1} = 210/h$  Mpc, and considered also the case of  $R_b = 120/h$  Mpc and  $R_{b1} = 140/h$  Mpc for comparison.

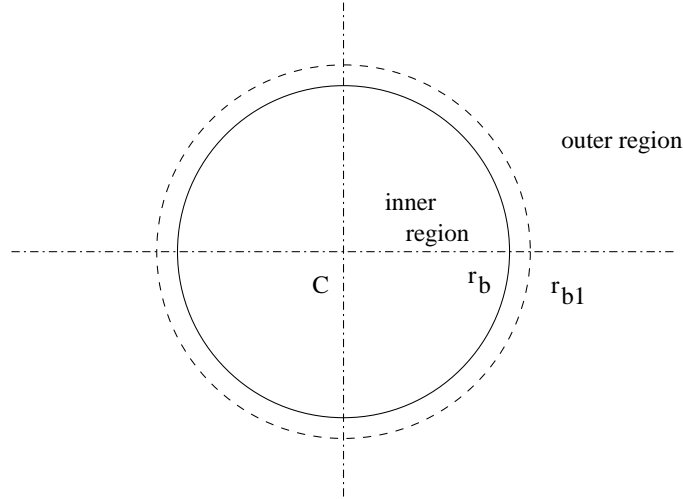


Fig. 2. Two regions and the boundary. Solid and dotted curves denote the surfaces with  $r = r_b$  and  $r = r_{b1}$ , respectively.

From the viewpoint of our models with a local void, the above model parameters are for the outer region ( $r > r_b$ ) and correspond to  $(\Omega_0^{\text{II}}, \lambda_0^{\text{II}}, h^{\text{II}})$  in the previous papers,<sup>10), 13)</sup> where  $H_0^{\text{II}} = 100h^{\text{II}} \text{ km s}^{-1} \text{ Mpc}^{-1}$ . As a result of simulations the parameters  $(\Omega_0^{\text{I}}, \lambda_0^{\text{I}}, h^{\text{I}})$  in the inner region are derived as their average values in the following:

$$H_0^{\text{I}} \equiv H_0^{\text{II}} + \left( \sum_{i \in I_*} v_{(i)} / r_{(i)} \right) / N_* \quad (3.2)$$

and  $\lambda_0^{\text{I}} \equiv \frac{1}{3} \Lambda / (H_0^{\text{I}})^2$ , where we take the summation for the set  $I_*$  of particles included in the region of  $r_l < r < r_b$  ( $r_l \sim 0.2r_b$ ), so as to avoid the disturbances near the origin and the boundary.  $N_*$  is the particle number in this region, and  $v_{(i)}$  and  $r_{(i)}$  are the radial velocities and radii of the  $i$ -th particles, where  $v_{(i)} \equiv (\sum_{k=1}^3 v_{(i)}^k x_{(i)}^k) / r_{(i)}$ .

For the particles which were initially in the inner region, the observed positions (in the redshift-space) are different from those represented by the background coordinates (in the real-space). To take the average velocity (in the inner region) into account, we define another coordinates (average comoving coordinates)  $\bar{x}^k$  ( $k = 1, 2, 3$ ):

$$\bar{x}^k = x^k \times \begin{cases} H_0^{\text{I}} / H_0^{\text{II}} & \text{for } r < r_b, \\ \left[ 1 + \left( \frac{H_0^{\text{I}}}{H_0^{\text{II}}} - 1 \right) \left( \frac{1}{r_b} - \frac{1}{r_{b1}} \right) / \left( \frac{1}{r} - \frac{1}{r_{b1}} \right) \right] & \text{for } r_b \leq r < r_{b1}, \end{cases} \quad (3.3)$$

and  $\bar{x}^k = x^k$  for  $r > r_{b1}$ . This coordinate system corresponds not only to the outer comoving one, but also the inner comoving one with respect to the mean motions. Using the volume  $V_* = \frac{4}{3} \pi a_0^3 (r_b^3 - r_l^3) (H_0^{\text{I}} / H_0^{\text{II}})^3$  in this coordinates, the density parameter in the inner region is defined as

$$\Omega_0^{\text{I}} \equiv \frac{3\pi G}{3(H_0^{\text{I}})^2} \frac{MN_*}{V_*}. \quad (3.4)$$

These values in the above three cases are shown in Table I together with  $d$  and  $R_b$ . The values of  $d$  were chosen so as to obtain  $\Omega_0^{\text{I}} \sim 0.3$  for three sets of  $(\Omega_0^{\text{II}}, \lambda_0^{\text{II}})$ . By comparing the case  $R_b h = 180$  and the case  $R_b h = 120$ , it is found to be not essential how to select the position of the boundary.

Table I. Inner model parameters determined statistically for the given outer model parameters  $(\Omega_0, \lambda_0, h) = (\Omega_0^{\text{II}}, \lambda_0^{\text{II}}, h^{\text{II}})$ .  $d$  is a constant expansion factor and  $R_b$  is the radial distance between the center C and the boundary.  $\Omega_b$  is the present baryon density parameter ( $\propto \Omega_0$ ).

$\Omega_0^{\text{II}} \lambda_0^{\text{II}} h^{\text{II}}$	$d$	$R_b h$ Mpc	$\Omega_0^{\text{I}} \lambda_0^{\text{I}} h^{\text{I}}$	$\Omega_b^{\text{I}} (h^{\text{II}})^2 / \Omega_b^{\text{I}} (h^{\text{I}})^2$
1.0 0.0 0.50	0.022	180	0.38 0.00 0.576	1.98
1.0 0.0 0.50	0.022	120	0.39 0.00 0.574	1.98
1.0 0.0 0.50	0.030	180	0.32 0.00 0.594	2.21
0.6 0.0 0.60	0.040	180	0.29 0.00 0.693	1.55
0.6 0.4 0.60	0.040	180	0.29 0.29 0.694	1.55

The distribution of dark-matter particles at present epoch is shown in Fig. 3 as an example for the model parameter set (1.0, 0.0, 0.5), where the particles in  $-3 \text{ Mpc} \leq a_0 x^3 \leq 3 \text{ Mpc}$  were plotted. The corresponding distributions of particles in  $\bar{x}^k$  coordinates are shown in Fig. 4. It is found that at present epoch the (dark-matter) particles in the inner region near the boundary seem to have been mixed with those in the outer region and so their distributions are much complicated near the boundary in the outer region.

#### §4. Theoretical two-point correlations

In this section the two-point correlations ( $\xi$ ) are derived in the numerical models given in the previous section. Their values in the inner region with  $r < r_b$  and the



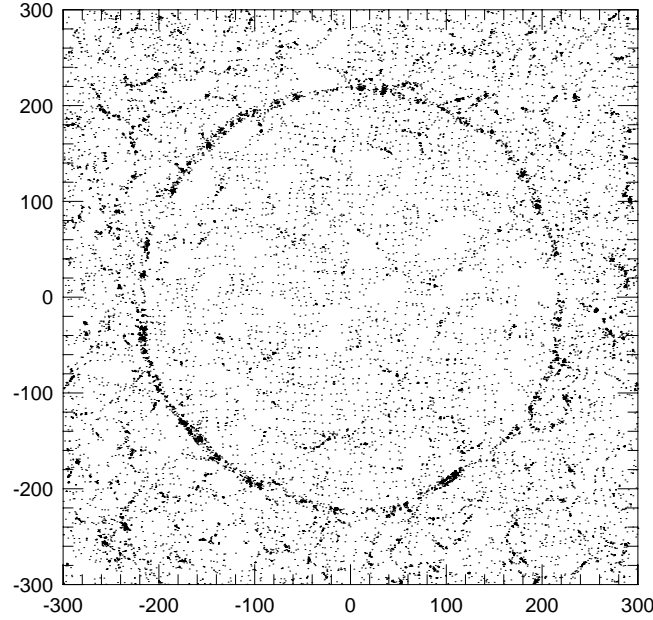


Fig. 3. The distribution of dark-matter particles in the  $(a_0 x^1, a_0 x^2)$  plane at present epoch in the case  $(\Omega_0^{\text{II}}, \lambda_0^{\text{II}}) = (1, 0)$  and  $R_b h = 180$  Mpc. The length is  $600/h$  Mpc and the width is  $6/h$  Mpc.

outer region with  $r_p > r \gg r_{b1}$  have simple behaviors, but they are complicated in the intermediate region ( $r_b < r < r_{b1}$ ), because the uncorrelated particles are mixed there. Here the correlations ( $\xi_i$  and  $\xi_o$ ) in the inner and outer regions, respectively, were calculated for the particle positions in the average comoving coordinates ( $\bar{x}^k$ ) in various cases with  $R_b h = 180$  Mpc which were treated in the previous sections. and they were identified in the form  $\xi = (r_0/R)^\gamma$  with  $\gamma = 1.7$  to derive the correlation lengths  $r_0$ . The result is shown in Table II.

Table II. Correlation lengths and the ratios of two-point correlations in the two regions of the models with  $R_b h = 180$  Mpc.  $h = h^{\text{II}}$

$\Omega_0^{\text{II}}$	$\lambda_0^{\text{II}}$	$h^{\text{I}}/h^{\text{II}}$	$r_0^{\text{II}}h$	$r_0^{\text{I}}h$	$\xi^{\text{I}}/\xi^{\text{II}}$	$\Omega_0^{\text{II}}h^{\text{II}}/(\Omega_0^{\text{I}}h^{\text{I}})$
1.0	0.0	1.152	5.2	4.2	1.5	2.3
1.0	0.0	1.188	5.6	3.8	2.1	2.6
0.6	0.0	1.155	6.5	5.0	1.6	1.8
0.6	0.4	1.156	5.4	3.9	1.8	1.8

It is found from this result that the ratio  $\xi_o/\xi_i$  is about 2.0 in the case with  $\Omega_0^{\text{II}} = 1.0$ ,  $\lambda_0^{\text{II}} = 0.0$ ,  $h^{\text{I}}/h^{\text{II}} = 1.188$ , and in the other cases it is somewhat smaller. Thus the situation that the ratio of correlations for dark-matter particles is larger than 1.5, is common to these models with a local void. Here we are going

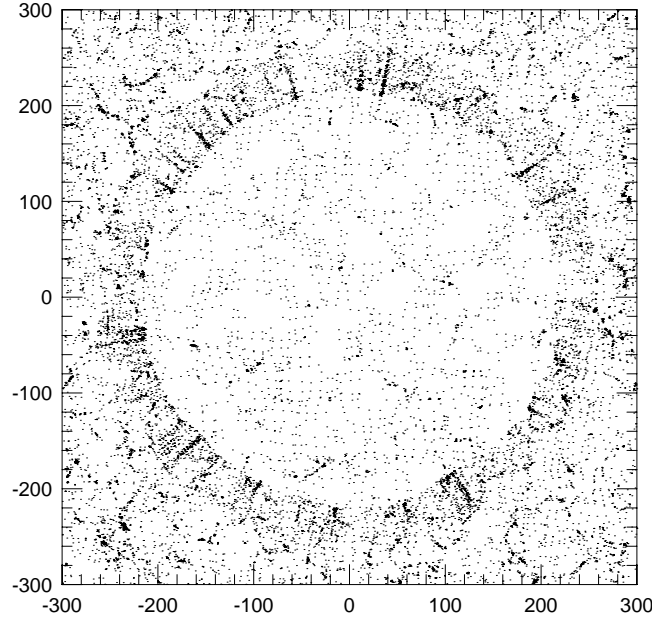


Fig. 4. The distribution of dark-matter particles in the  $(a_0\bar{x}^1, a_0\bar{x}^2)$  plane at present epoch in the case  $(\Omega_0^{\text{II}}, \lambda_0^{\text{II}}) = (1, 0)$  and  $R_b h = 180$  Mpc. The length is  $600/h$  Mpc and the width is  $6/h$  Mpc.

to compare this with the ratio for galaxies, but in general the clustering of galaxies depends not only on the background model, but also on their luminosity through the bias effect. For galaxies with comparatively low luminosity, however, the bias effect on the clustering seems to be small, and the ratio for dark matter may be equal to that for galaxies with  $M_{bJ} = -18 \sim -21$ . So it can be concluded that the theoretical ratio  $(\xi_o/\xi_i)$  can explain the change in the observed ratio for galaxies with  $M_{bJ} = -18 \sim -21$ .

Now let us consider the power spectra in the two regions. If the spatial scales are  $\ll r_b$  or  $\gg r_b$ , we can treat the power spectrum in each region, as that in a homogeneous model with a fitting formula ( $i = \text{I and II}$ ):

$$P_i(k) \propto k \left[ \frac{\ln(1 + 2.34q_i)}{2.34q_i} \right]^2 [1 + 3.89q_i + (16.1q_i)^2 + (5.46q_i)^3 + (6.71q_i)^4]^{-1/2}, \quad (4.1)$$

where  $q_i = k(h^i)^{-1}/\Gamma_i$  and the shape parameter is  $\Gamma_i \equiv \Omega_0^i h^i \exp[-\Omega_B^i (1 + \sqrt{2h^i/\Omega_0^i})]$  depending on the baryon density.<sup>42)</sup> In the outer region we can derive  $\Omega_0^{\text{II}} h^{\text{II}}$  from the measurements of CMB anisotropies, but at present we have the rough values  $\Omega_0^{\text{II}} h^{\text{II}} = 0.3 \sim 0.5$ , which are obtained as those with weak prior from Boomerang, DASI and MAXIMA experiments.<sup>5), 7), 9)</sup> In the inner region also we can roughly

estimate  $\Omega_0^I h^I$  from Peacock and Dodds's treatment<sup>43)</sup> in which they derived the reconstructed linear data of density contrasts for galaxies and clusters. Their data for  $k/h < 0.02 \text{ Mpc}^{-1}$  belong to our outer region and have comparatively large uncertainty, so that, by putting larger weights to data for  $k/h > 0.03 \text{ Mpc}^{-1}$ , we obtain  $\Omega_0^I h^I = 0.2 \sim 0.25$ . So we have the observational ratio  $\Omega_0^I h^I / (\Omega_0^I h^I) = 1.0 \sim 2.5$  at present.

In our models, on the other hand, we have the ratios shown in the last column of Table II in the cases (1), (2) and (3), and so our models are found to correspond to the case with comparatively large ratios.

### §5. Bulk flows in the inner region

If we observed at the center C, the average velocity field would be isotropic and the direction of velocities of particles is radial at each point in the inner region. From the off-center observer O (being a realistic observer), however, the average velocity field is anisotropic and the non-radial component is found to be significant, when each velocity( $\vec{v}$ ) in the inner region is divided into the component ( $v_r$ ) in the radial direction  $O \rightarrow A$  and the component ( $v_p$ ) in the direction  $C \rightarrow O$  as

$$\vec{v} = v_r \vec{l} + v_p \vec{n}. \quad (5.1)$$

Here  $\vec{l}$  and  $\vec{n}$  are the unit vectors in the directions of  $O \rightarrow A$  and  $C \rightarrow O$ , respectively (see Fig. 5), and we have

$$v_r = \left[ \vec{v} \vec{l} - (\vec{v} \vec{n})(\vec{l} \vec{n}) \right] / \left[ 1 - (\vec{l} \vec{n})^2 \right], \quad (5.2)$$

and

$$v_p = \left[ \vec{v} \vec{n} - (\vec{v} \vec{l})(\vec{n} \vec{l}) \right] / \left[ 1 - (\vec{l} \vec{n})^2 \right]. \quad (5.3)$$

Then the mean physical value  $V_p$  for  $v_p$  is defined by

$$V_p \equiv a_0 \left( \sum_{i \in I_*} v_{p(i)} \right) / N_* \quad (5.4)$$

where  $i$  is the particle index and  $N_*$  is the particle number in  $I_*$  set. This value depends on the model parameters and is proportional to the distance  $R_{co} (\equiv a_0 r_{co})$  from C to O. By choosing O in  $N_0$  different directions with equal  $R_{co}$ , moreover, we can derive the  $N_0$  independent values of  $V_p$ . Using them we obtained the following average value of  $V_p$  and the dispersion ( $\sigma_p$ ) for  $N_0 = 6$ . Their values are shown in Table III for models with  $R_b = 180/h \text{ Mpc}$  and  $R_{co} = 50$  or  $60/h \text{ Mpc}$ , where  $h = h^I$ . The values of  $V_{\text{bulk}} \equiv (H_0^I - H_0^{II}) R_{co} = 100(h^I - h^{II}) R_{co}$  also are shown, and it is found that  $V_p$  is equal to  $V_{\text{bulk}}$ . In the inner region the average velocity field of galaxies is equal to that of dark matter, and so this velocity may correspond to the bulk flow of clusters with the velocity  $\sim 700 \text{ km s}^{-1}$  which was discovered by Hudson et al.<sup>11)</sup> and Willick<sup>12)</sup> and so all of models with a local void treated here are consistent with their observations for appropriate  $R_{co}$ .

Table III. Bulk velocities and their dispersions

$\Omega_0^{\text{II}}$	$\lambda_0^{\text{II}}$	$R_{co}h$ Mpc	$V_p$ km/s	$\sigma_p$ km/s	$V_{\text{bulk}}$ km/s
1.0	0.0	50	764.5	49.5	760
1.0	0.0	40	752.8	46.6	752
0.6	0.0	50	774.5	66.8	775
0.6	0.4	50	777.6	57.1	780

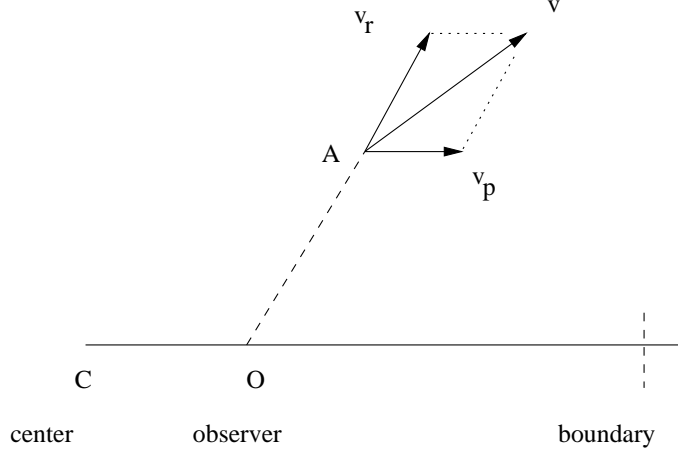


Fig. 5. Velocity vectors in the inner region.

For an off-center observer, CMB seems to be anisotropic. The dipole moment  $D$  was derived in Ref. <sup>13)</sup> and the dipole velocity  $V_D$  was found to be of the order of  $0.1V_p (\approx 70) \text{ km s}^{-1}$ , so that it may be part of the peculiar velocity  $\sim 500 \text{ km s}^{-1}$  of the Local Group towards the Attractor.

## §6. Baryon contents

From the observational studies of light elements it is found that in the remote past we have the values  $\Omega_b h^2 \cong 0.025$ , which is derived from the analysis of deuterium abundance in QSOs at  $z \sim 2$ . <sup>48), 49), 50)</sup> Moreover, the recent studies of CMB anisotropy suggest the similar content of baryons  $\Omega_b h^2 = 0.02 \sim 0.03$  <sup>5), 7)</sup>.

Next let us consider the baryon contents in our models with a void. Here it is assumed that dark matter and baryons are well mixed and so the ratio of the baryon density to the matter density is equal everywhere. Then in the case with  $(\Omega_0^{\text{I}}, \Omega_0^{\text{II}}) = (0.3, 1.0)$  and  $h^{\text{II}} = h^{\text{I}} \times 0.8$  in the inner (I) and outer (II) regions, we have  $\Omega_0^{\text{II}}/\Omega_0^{\text{I}} = 1.0/0.3$ , so that  $\Omega_0^{\text{II}}(h^{\text{II}})^2 = 2.1 \times \Omega_0^{\text{I}}(h^{\text{I}})^2$  and  $\Omega_b^{\text{II}}(h^{\text{II}})^2 = 2.1 \times \Omega_b^{\text{I}}(h^{\text{I}})^2$ . The ratios  $\Omega_b^{\text{II}}(h^{\text{II}})^2/\Omega_b^{\text{I}}(h^{\text{I}})^2$  for simulated models we treated here are shown in the last column of Table I. It is found from this Table that in models with  $\Omega_0^{\text{II}} = 1.0$  the ratio can be about 2, and in models  $\Omega_0^{\text{II}} = 0.6$  the ratios are somewhat smaller.

Using the above observational content in the outer region, accordingly, we obtain  $\Omega_b h^2$  is  $0.010 \sim 0.015$  in the inner region. As long as all inhomogeneities are produced adiabatically, the baryon/photon ratio ( $\eta$ ) is equal and constant ( $\simeq 7 \times 10^{-10}$ ) everywhere, so that at the very early stage with primordial nuclear reactions, the

photon number densities also were inhomogeneous, but at the present stage they have been equalized in both regions owing to the free propagation of photons.

If the so-called *crisis* of big-bang nucleosynthesis<sup>(44), (45)</sup> is true and  $\eta$  is really inhomogeneous (i.e.  $\eta \simeq 3 \times 10^{-10}$  in the inner region) in connection with the primordial abundance of Li<sup>7</sup>,<sup>(46), (47)</sup> it may be necessary in order to avoid the *crisis*, to invoke that the void was produced as a special large-scale structure including non-adiabatic perturbations.

## §7. Concluding remarks

In this paper we first considered galaxy formation in inhomogeneous models with a local void. The observed distribution of galaxies seems to be homogeneous, but we discussed there the possibility that the homogeneity may be an appearance brought by the complicated feedback processes of galaxy formation and evolution in the inhomogeneous distribution of dark matter halos. In order to clarify observationally the signs of the boundary of the void, then it is necessary to investigate the more details of galactic distributions, such as the distribution of active (colliding) galaxies and two-point correlations.

Next we derived numerical inhomogeneous models consisting of dark-matter particles with a spherical low-density (inner) region and studied the two-point correlations in the inner and outer regions. It was found that they can be consistent with the redshift dependence of observed correlations of low-luminosity galaxies. Moreover we derived the bulk flow found by the off-center observer, which corresponds to the observed large-scale bulk flow. Finally we studied the baryon contents and discussed a possibility to avoid the *crisis* of light elements.

In previous papers<sup>(13), (14), (15)</sup> I calculated luminosity and angular-diameter distances to derive  $[m, z]$  relation, and found that the distances in our models with a local void are similar to those in  $\Lambda$ -dominant homogeneous models in the redshift interval  $0 < z < z_m (\approx 1)$ . So in the observations using mainly the distances, such as the number-counts of galaxies and clusters, the theoretical relations  $N(m)$  in the above two different types of models are similar in the interval  $0 < z < z_m$ . Even if the observations on  $N(m)$  rule out the SCDM model ( $\Lambda = 0$ ),<sup>(51), (52)</sup> accordingly, our models with a local void and  $\Lambda = 0$  may be consistent with the observations in similar ways to the  $\Lambda$ -dominant homogeneous models.

At present it is well-known that we are in the low-density region ( $\Omega_0 \sim 0.3$ ), but the total matter density and baryon content in the remote region ( $z > 1$ ) are not so clear. From the observations of the anisotropy of CMB, we can constrain the model parameters and baryon content, but the recent results of Boomerang, DASI and MAXIMA experiments,<sup>(5), (7), (9)</sup> however, seem to be different and rather inconsistent with respect to the density parameter and the baryon content. So the precise measurement by the MAP satellite in near future is very important to determine the above values more accurately. If the additive data from SNIa with  $z > 1.5$  are moreover provided by the SNAP satellite and large telescopes like Subaru etc, the model parameters in the remote region will be much clearer.

## Acknowledgements

The author is grateful to Y. Suto and T. Sugimotohara for providing me with their useful tree code for my simulations. This work was supported by a Grant-in Aid for Scientific Research (No. 12440063) from the Ministry of Education, Science, Sports and Culture, Japan. He owes also to the YITP computer system for the numerical analyses.

## References

- [1] B. P. Schmidt, N. B. Suntzeff, M. M. Phillips, R. A. Schommer, A. Clocchiatti, R. P. Kirshner, P. Garnavich, P. Challis et al., *Astrophys. J.* **507** (1998), 46.
- [2] A. G. Riess, A. V. Filippenko, P. Challis, A. Clocchiatti, A. Diercks, P. M. Garnavich, R. L. Gilliland et al., *Astron. J.* **116** (1998), 1009.
- [3] A. G. Riess, A. V. Filippenko, W. Li and B. Schmidt, *Astron. J.* **118** (2000), 2668.
- [4] S. Perlmutter, G. Aldering, G. Goldhaber, R. A. Knop, P. Nugent, D. E. Groom, P. G. Castro, S. Deustua, et al., *Astrophys. J.* **517** (1999), 565.
- [5] A. E. Lange, et al., *Phys. Rev.* **D63** (2001), 042001.
- [6] A. T. Lee, et al., *Astrophys. J.* **561** (2001), L1.
- [7] R. Stomper, et al., *Astrophys. J.* **561** (2001), L7.
- [8] N. W. Halverson et al., *astro-ph/0104489*.
- [9] C. Pryke et al., *astro-ph/0104490*.
- [10] K. Tomita, *Astrophys. J.* **529** (2000), 26.
- [11] M. J. Hudson, R. J. Smith, J. R. Lucey, D. J. Schlegel and R. L. Davies, *Astrophys. J.* **512** (1999), L79.
- [12] J. A. Willick, *Astrophys. J.* **522** (1999), 647.
- [13] K. Tomita, *Astrophys. J.* **529** (2000), 38.
- [14] K. Tomita, *Mon. Not. R. Astron. Soc.* **326** (2001), 287.
- [15] K. Tomita, *Prog. Theor. Phys.* **106** (2001), 929, *astro-ph/0104141*.
- [16] A. G. Riess et al., *astro-ph/0104455*.
- [17] S. D. M. White and M. J. Rees, *Mon. Not. R. Astron. Soc.* **183** (1978), 341.
- [18] S. D. M. White and C. S. Frenk, *Astrophys. J.* **379** (1991), 52.
- [19] G. Kauffmann, B. Guiderdoni and S. D. M. White, *Mon. Not. R. Astron. Soc.* **267** (1994), 981.
- [20] S. Cole et al., *Mon. Not. R. Astron. Soc.* **271** (1994), 781.
- [21] S. Cole et al., *Mon. Not. R. Astron. Soc.* **319** (2000), 168.
- [22] R. S. Somerville and J. R. Primack, *Mon. Not. R. Astron. Soc.* **310** (1999), 1087.
- [23] G. Kauffmann, A. Nusser and M. Steinmetz, *Mon. Not. R. Astron. Soc.* **286** (1997), 795.
- [24] G. Kauffmann, J. M. Colberg, A. Diaferi and S. D. M. White, *Mon. Not. R. Astron. Soc.* **303** (1999), 188.
- [25] A. J. Benson et al., *Mon. Not. R. Astron. Soc.* **000** (2001), 000, *astro-ph/0103092*.
- [26] R. S. Somerville et al., *Mon. Not. R. Astron. Soc.* **320** (2001), 289.
- [27] R. Cen and J. Ostriker, *Astrophys. J.* **417** (1993), 404.
- [28] N. Katz, D. H. Weinberg and L. Herquist, *Astrophys. J. Suppl.* **105** (1996), 19.
- [29] C. S. Frenk et al., *Astrophys. J.* **472** (1996), 460.
- [30] S. T. Kay et al., *Mon. Not. R. Astron. Soc.* **330** (2002), 113.
- [31] A. A. Thoul and D. H. Weinberg, *Astrophys. J.* **465** (1996), 608.
- [32] G. Efstathiou, *Mon. Not. R. Astron. Soc.* **256** (1992), 43p.
- [33] M. Nagashima, N. Gouda and N. Sugiura, *Mon. Not. R. Astron. Soc.* **305** (1999), 449.
- [34] G. Efstathiou, *Mon. Not. R. Astron. Soc.* **317** (2000), 697.
- [35] C. Marinoni, P. Monaco, G. Giuricin and B. Costantini, *Astrophys. J.* **521** (1999), 50.
- [36] R. O. Marzke, L. N. da Costa, P. S. Pellegrini, C. N. A. Willmer and M. J. Geller, *Astrophys. J.* **503** (1998), 617.
- [37] S. Folkes, S. Ronen, I. Price, O. Lahav, M. Colless, S. Maddox, K. Deeley, K. Glazebrook et al., *Mon. Not. R. Astron. Soc.* **308** (1999), 459.
- [38] E. Zucca, G. Zamorani, G. Vettolani, A. Cappi, R. Merighi, M. Mignoli, H. MacGillivray,

- C. Collins et al., *Astron. Astrophys.* **326** (1997), 477.
- [39] D. S. Madwick et al., astro-ph/0107197.
- [40] P. Norberg et al., *Mon. Not. R. Astron. Soc.* **328** (2001), 64.
- [41] I. Zehavi et al., astro-ph/0106476.
- [42] N. Sugiyama, *Astrophys. J. Suppl.* **100** (1995), 281.
- [43] J. A. Peacock and S. J. Dodds, *Mon. Not. R. Astron. Soc.* **267** (1994), 1020.
- [44] K. A. Olive and D. N. Schramm, *Nature* **360** (1992), 439.
- [45] G. Steigman, *Critical Dialogue in Cosmology* (Proc. Princeton University Conference), 1.
- [46] K. A. Olive, astro-ph/0009475.
- [47] S. G. Ryan et al., *Astrophys. J.* **530** (2000), L57.
- [48] O'Meara et al., *Astrophys. J.* **552** (2001), 718.
- [49] M. Pettini and D. V. Bowen, *Astrophys. J.* **560** (2001), 41.
- [50] S. Burles, K. M. Nollett and M. S. Turner, *Astrophys. J.* **552** (2001), L1.
- [51] Y. Yoshii and B. A. Peterson, *Astrophys. J.* **444** (1995), 15.
- [52] T. Totani et al., *Astrophys. J.* **550** (2001), L137.